Clinical Chemistry 62:1
157–169 (2016)

High-Resolution Mass Spectrometry for Characterizing the Metabolism of Synthetic Cannabinoid THJ-018 and Its 5-Fluoro Analog THJ-2201 after Incubation in Human Hepatocytes

Xingxing Diao,[1] Ariane Wohlfarth,[1] Shaokun Pang,[2] Karl B. Scheidweiler,[1] and Marilyn A. Huestis[1*]

BACKGROUND: Despite increasing prevalence of novel psychoactive substances, no human metabolism data are currently available, complicating laboratory documentation of intake in urine samples and assessment of the drugs' pharmacodynamic, pharmacokinetic, and toxicological properties. In 2014, THJ-018 and THJ-2201, synthetic cannabinoid indazole analogs of JWH-018 and AM-2201, were identified, with the National Forensic Laboratory Information System containing 220 THJ-2201 reports. Because of numerous adverse events, the Drug Enforcement Administration listed THJ-2201 as Schedule I in January 2015.

METHODS: We used high-resolution mass spectrometry (HR-MS) (TripleTOF 5600$^+$) to identify optimal metabolite markers after incubating 10 μmol/L THJ-018 and THJ-2201 in human hepatocytes for 3 h. Data were acquired via full scan and information-dependent acquisition triggered product ion scans with mass defect filter. In silico metabolite predictions were performed with MetaSite and compared with metabolites identified in human hepatocytes.

RESULTS: Thirteen THJ-018 metabolites were detected, with the major metabolic pathways being hydroxylation on the *N*-pentyl chain and further oxidation or glucuronidation. For THJ-2201, 27 metabolites were observed, predominantly oxidative defluorination plus subsequent carboxylation or glucuronidation, and glucuronidation of hydroxylated metabolites. Dihydrodiol formation on the naphthalene moiety was observed for both compounds. MetaSite prediction matched well with THJ-018 hepatocyte metabolites but underestimated THJ-2201 oxidative defluorination.

CONCLUSIONS: With HR-MS for data acquisition and processing, we characterized THJ-018 and THJ-2201 metabolism in human hepatocytes and suggest appropriate markers for laboratories to identify THJ-018 and THJ-2201 intake and link observed adverse events to these new synthetic cannabinoids.

Synthetic cannabinoids (SCs) interact with endogenous cannabinoid receptors and elicit cannabimimetic effects similar to those of Δ^9-tetrahydrocannabinol *(1, 2)*. SC[3] abuse causes serious toxicities, including acute kidney injury, myocardial infarction, and death *(3, 4)*. Despite these health hazards, SC intake persists. Many SCs (e.g., JWH018, JWH-073, AKB48, and XLR-11) have been scheduled in the US, Japan, and most European countries; however, more structurally diverse compounds continuously emerge.

Two new SCs, THJ-018 [1-naphthalenyl(1-pentyl-1H-indazol-3-yl)-methanone] and its 5-fluoro analog, THJ-2201 [(1-(5-fluoropentyl)-1H-indazol-3-yl)(naphthalen-1-yl)methanone] (Fig. 1), were found in the US, Japan, and Russia in 2014 *(5–8)*. The indole core of JWH-018 and AM2201 is replaced by indazole in THJ-018 and THJ-2201. The National Forensic Laboratory Information System has detailed 220 THJ-2201 reports since January 2014 *(7)*. Although no THJ-018 prevalence data are available, drug-user forums suggested increasing popularity for both analogs *(9)*. In January 2015, THJ-2201 became a Schedule I compound in the US *(7)*; THJ-018 and THJ-2201 were scheduled in Japan in August 2014 *(10)*. Currently, THJ-018 and THJ-2201 pharmacological data are unavailable; however,

[1] Chemistry and Drug Metabolism, Intramural Research Program, National Institute on Drug Abuse, NIH, Baltimore, MD; [2] SCIEX, Redwood City, CA.
* Address correspondence to this author at: Chemistry and Drug Metabolism, IRP, National Institute on Drug Abuse, NIH, 251 Bayview Blvd, Suite 200 Room 05A721, Baltimore, MD 21224. Fax 443-740-2823; e-mail mhuestis@intra.nida.nih.gov.
Received May 17, 2015; accepted July 21, 2015.
Previously published online at DOI: 10.1373/clinchem.2015.243535

[3] Nonstandard abbreviations: SC, synthetic cannabinoid; THJ-018, 1-naphthalenyl(1-pentyl-1H-indazol-3-yl)-methanone; THJ-2201, (1-(5-fluoropentyl)-1H-indazol-3-yl)(naphthalen-1-yl)methanone; HR-MS, high-resolution mass spectrometry; HLM, human liver microsome; NPS, novel psychoactive substance; KHB, Krebs-Henseleit buffer; IDA, information-dependent acquisition; MDF, mass defect filter; CYP450, cytochrome P450; $CL_{int,\ micr}$, microsomal intrinsic clearance; CL_{int}, intrinsic clearance; CL_H, hepatic clearance; ER, extraction ratio.

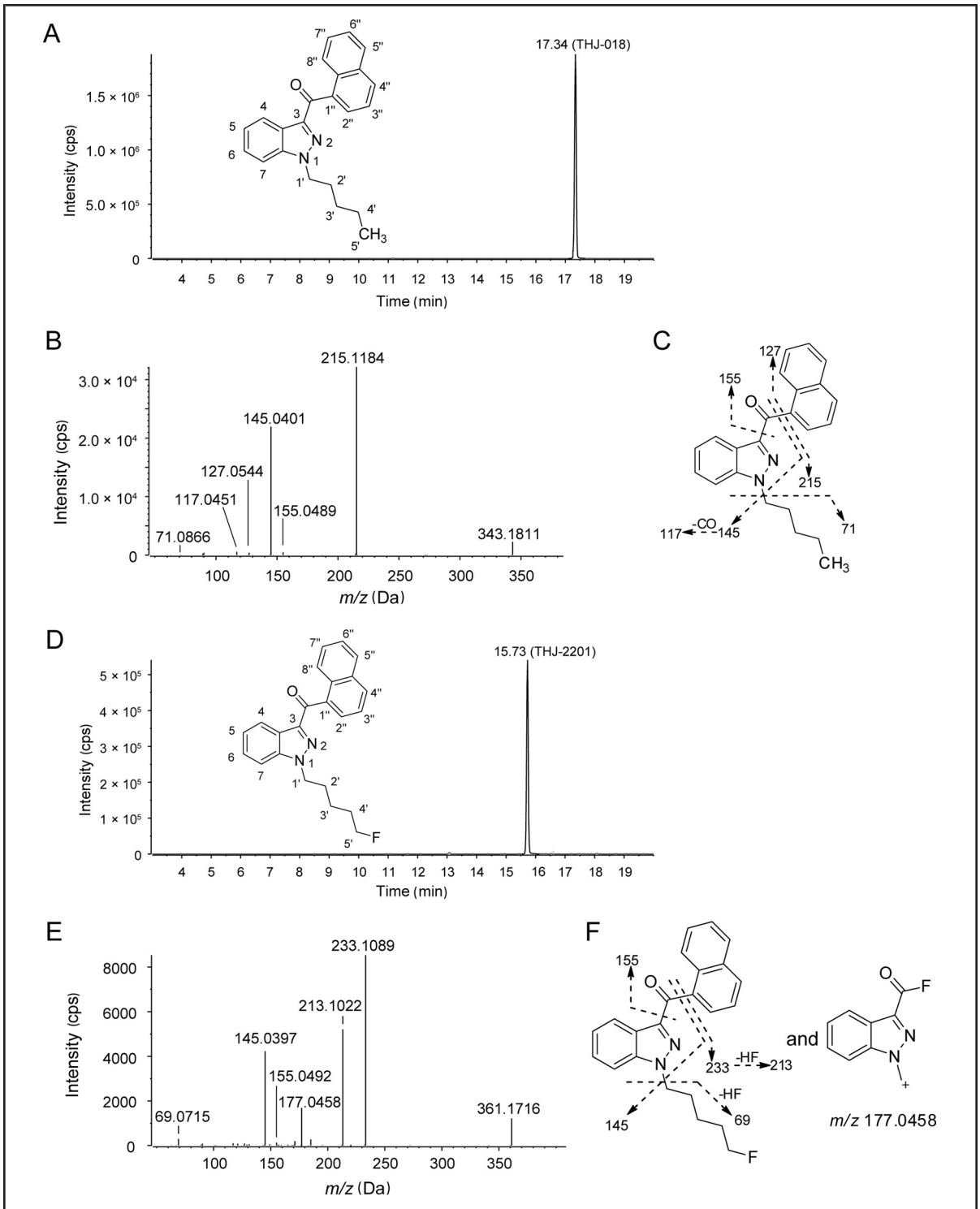

Fig. 1. THJ-018, *m/z* 343.1811, extracted ion chromatogram (A) (structure as inset), product ion spectrum (B), and proposed fragmentation pattern (C). THJ-2201, *m/z* 361.1716, extracted ion chromatogram (D) (structure as inset), product ion spectrum (E), and proposed fragmentation pattern (F).

Carbons were numbered for metabolite identification.

they should possess similar affinity to cannabinoid receptors as JWH-018 and AM-2201 *(11)*. Adverse reactions, such as kidney pains, muscle spasms, and paranoia, were reported on drug-user forums *(9)*.

All investigated SCs undergo extensive metabolism in humans, with little to no parent compound excreted in urine *(11–13)*, complicating detection, since metabolites are initially unknown. Because urine is the most common matrix in clinical, antidoping, and military drug testing, characterizing THJ-018 and THJ-2201 metabolism is essential for developing effective urine screening methods. THJ-018 and THJ-2201 metabolism is unknown. However, JWH-018 and AM-2201 metabolism have been intensively studied *(12, 14–16)*. JWH-018 undergoes monohydroxylation on the naphthalene, indole, and pentyl chain, as well as carboxylation *(14, 15)*. In contrast, AM-2201 primarily undergoes oxidative defluorination and subsequent carboxylation *(12, 16)*.

We used high-resolution mass spectrometry (HR-MS) for data acquisition instead of traditional unit–resolution MS. HR-MS facilitates the interpretation of fragment formula, accomplishing all requisite metabolite identification tasks with improved productivity and quality *(17)*. Traditional unit–resolution MS requires multiple injections with different acquisition methods to identify metabolites, and data analysis is more time-consuming and less reliable because of uncertainty of fragment formula.

Human hepatocytes were chosen over human liver microsomes (HLMs) because hepatocytes contain all endogenous drug-metabolizing enzymes and essential cofactors *(18)*. Metabolites identified with human hepatocytes can serve as useful markers for identifying novel SCs *(19)*. Recent increases in drug-related emergency visits have been linked to new novel psychoactive substances (NPSs) *(20)*. Identification of urinary metabolites for documenting NPS intake is critical for determining the cause of adverse events.

The objectives of this study were to characterize THJ-018 and THJ-2201 metabolism, identify optimal markers to document SC intake, link observed adverse events to causative substances, and provide reference standard manufacturers with the most critical metabolites for synthesis efforts.

Materials and Methods

CHEMICALS AND REAGENTS

We purchased THJ-018 and THJ-2201 from Cayman Chemicals. Cryopreserved human hepatocytes (10-donor pool), Gro CP buffer, and Krebs-Henseleit buffer (KHB) were obtained from BioreclamationIVT, and LC-MS grade water, formic acid, and acetonitrile from Fisher Scientific.

METABOLIC STABILITY IN HLMs

The metabolic stability assay is shown in Supplemental Methods and Data, which accompanies the online version of this article at http://www.clinchem.org/content/vol62/issue1.

HEPATOCYTE INCUBATION

Cryopreserved human hepatocytes were thawed in a 37 °C water bath, washed twice with Gro CP medium and KHB, and assessed with Trypan blue (0.4%, vol/vol) to ensure >80% viability. THJ-018 and THJ-2201 were dissolved in methanol and diluted in KHB buffer at final incubation concentrations of 10 μmol/L. Human hepatocytes (0.5 mL; 1.0×10^6 cells/mL) were incubated in a 24-well plate at 37 °C. Reactions were terminated with 500 μL ice-cold acetonitrile after 0 and 3 h, and samples were stored at −80 °C until analysis. Diclofenac was incubated to ensure hepatocyte metabolic activity by monitoring metabolism to 4′-hydroxydiclofenac and acyl-β-D-glucuronide diclofenac.

HEPATOCYTE SAMPLE PREPARATION

Hepatocyte samples were thawed, vortex-mixed, and clarified via centrifugation (15 000*g*, 4 °C, 5 min). The supernatant was diluted 1:4 in 0.1% formic acid in water (mobile phase A), and 25 μL was injected.

CHROMATOGRAPHIC CONDITIONS

The Shimadzu HPLC system consisted of 2 LC-20AD_{XR} pumps, a DGU-20A3R degasser, a SIL-20AC_{XR} autosampler, and a CTO-20A column oven. We performed chromatographic separation with a Kinetex™ C18 column (100 × 2.1 mm internal diameter, 2.6 μm) fitted with a KrudKatcher Ultra HPLC inline filter (0.5 μm × 0.1 mm internal diameter) (Phenomenex). Gradient elution (at a flow rate of 0.3 mL/min) was 10% of mobile phase B (0.1% formic acid in acetonitrile) for 2 min, ramping to 95% B at 20 min, holding until 22 min, and reequilibrating at 10% B for 3 min. Column and autosampler temperatures were 40 and 4 °C, respectively.

DATA ACQUISITION AND PROCESSING

Data acquisition was performed with Analyst TF (V1.6) on a 5600$^+$ TripleTOF® mass spectrometer (SCIEX). The MS method consisted of TOF full scan and information-dependent acquisition (IDA) with positive electrospray ionization. Source parameters were temperature, 500 °C; ion spray voltage, 5500 V; gas 1, 50 psi; gas 2, 50 psi; curtain gas, 45 psi; declustering potential, 80 V; and collision energy, 10 eV. For IDA, multiple mass defect filters (MDFs) and dynamic background subtraction were used; spectra exceeding 100 cps were

selected for dependent MS/MS scan; isotopes within 3 Da were excluded; mass tolerance was 50 mDa; and collision energy was set to 35 (15) eV.

We used MetabolitePilot™ (V1.5; SCIEX) with different algorithms including common product ion, neutral loss, MDF, predicted biotransformation, and generic LC peak-finding. LC peak, MS, and MS/MS intensity thresholds were set at 200, 50, and 25 cps, respectively. Additional details are shown in online Supplemental Methods and Data.

IN SILICO PREDICTION

MetaSite software (V5; Molecular Discovery) predicts cytochrome P450 (CYP450) and flavin-containing monooxygenase catalyzed phase I metabolism. Potential THJ-018 and THJ-2201 metabolites were predicted and compared with hepatocyte metabolites. First-generation metabolites with 100% probability scores were reprocessed to obtain second-generation metabolites.

Results

METABOLIC STABILITY IN HLMs

For THJ-018, in vitro half-life ($T_{1/2}$) was 19.2 (0.11) min, and in vitro microsomal intrinsic clearance ($CL_{int,\ micr}$) was 0.036 $mL \cdot min^{-1} \cdot mg^{-1}$, which was scaled to whole liver dimensions yielding an intrinsic clearance (CL_{int}) of 34.2 $mL \cdot min^{-1} \cdot kg^{-1}$. Without considering plasma protein binding and with a simplified Rowland equation *(21)*, we calculated the predicted human hepatic clearance (CL_H) as 12.6 $mL \cdot min^{-1} \cdot kg^{-1}$ and an extraction ratio (ER) of 0.63. For THJ-2201, in vitro $T_{1/2}$, microsomal $CL_{int,\ micr}$, CL_{int}, CL_H, and ER were 10.8 (0.01) min, 0.064 $mL \cdot min^{-1} \cdot mg^{-1}$, 60.8 $mL \cdot min^{-1} \cdot kg^{-1}$, 15.1 $mL \cdot min^{-1} \cdot kg^{-1}$, and 0.75, respectively.

THJ-018 AND THJ-2201 FRAGMENTATION

Fig. 1, A–C, shows the THJ-018 extracted ion chromatogram and its product ion spectrum. The peak fragment *m/z* 215.1184 is generated via neutral loss of naphthalene; further cleaving of the pentyl chain yields *m/z* 145.0401. Fragments *m/z* 155.0489, 127.0544, and 71.0866 represent the naphthalene acylium ion, naphthalene, and pentyl chain, respectively.

As shown in Fig. 1, D–F, THJ-2201 produces major fragments at *m/z* 233.1089 and 145.0397, corresponding to the indazole with and without pentyl chain. Neutral loss of hydrogen fluoride from *m/z* 233.1089 generates *m/z* 213.1022. Minor fragments *m/z* 155.0491 and 69.0715 represent the naphthalene and pentyl chain without hydrogen fluoride, respectively; *m/z* 177.0458 is formed by fluorine rearrangement.

THJ-018 METABOLITES IN HEPATOCYTES

We identified 13 THJ-018 metabolites in hepatocyte samples (Fig. 2; Table 1). Metabolites were named in the order of retention time. No reference standards for confirmation of the tentative metabolites were commercially available.

MAJOR THJ-018 METABOLITES

On the basis of peak areas, major metabolites were 5′-OH-THJ-018 glucuronide (M4), 4′-OH-THJ-018 glucuronide (M3), 4′-carbonyl-THJ-018 (M11), 4′-OH-THJ-018 (M9), pent-1′-enyl-THJ-018 (M13), and hydroxylated 4′-OH-THJ-018 (M1). Their product ion spectra and proposed fragmentation are shown in Fig. 3, A–E. Product ion spectra of other metabolites are shown in online Supplemental Fig. 1.

5′-HYDROXYLATION AND FURTHER CARBOXYLATION AND GLUCURONIDATION

Three 5′-hydroxylation–related metabolites were observed (M8, M7, and M4). M8 shared fragments *m/z* 155.0480, 145.0399, and 127.0534 with THJ-018; *m/z* 231.1124 was 15.9940 Da larger than *m/z* 215.1184 of THJ-018, suggesting pentyl chain hydroxylation. M8 displayed the same retention time and fragmentation profile as F26 of THJ-2201, 5′-OH-THJ-018 (Fig. 3J).

M8 carboxylation yielded THJ-018 pentanoic acid (M7), and glucuronidation formed 5′-OH-THJ-018 glucuronide (M4). M7 and M4 corresponded to THJ-2201 metabolites F25 and F18 (Fig. 3, H–I), respectively, which were second-generation metabolites of F26. Neutral loss of HCOOH and presence of *m/z* 227.0818 and 217.0949 indicated that M7 was a carboxylic acid (Fig. 3I). In M4, neutral loss of the glucuronide generated *m/z* 359.1766 and other fragments were the same as M8, suggesting that M4 was 5′-OH-THJ-018 glucuronide.

4′-HYDROXYLATION AND FURTHER OXIDATION AND GLUCURONIDATION

4′-Hydroxylation was another major metabolic pathway, producing 5 metabolites (M9, M3, M11, M1, and M2). M9 coeluted with M8 (5′-OH-THJ-018) and shared the same product ions (Fig. 3C). We propose M9 as 4′-OH-THJ-018 because ω-hydroxylation and ω-1-hydroxylation were usually the primary biotransformations for drugs with aliphatic side chains and displayed similar physicochemical properties *(22–24)*. This phenomenon also was observed for 5′-OH-JWH-018 and 4′-OH-JWH-018 *(11)*. Glucuronidation of M9 forms M3 (4′-OH-THJ-018 glucuronide) (Fig. 3B), coeluting with M4 (5′-OH-THJ-018 glucuronide) owing to close physicochemical properties.

4′-OH-THJ-018 (M9) underwent further dehydrogenation to 4′-carbonyl-THJ-018 (M11). M11 frag-

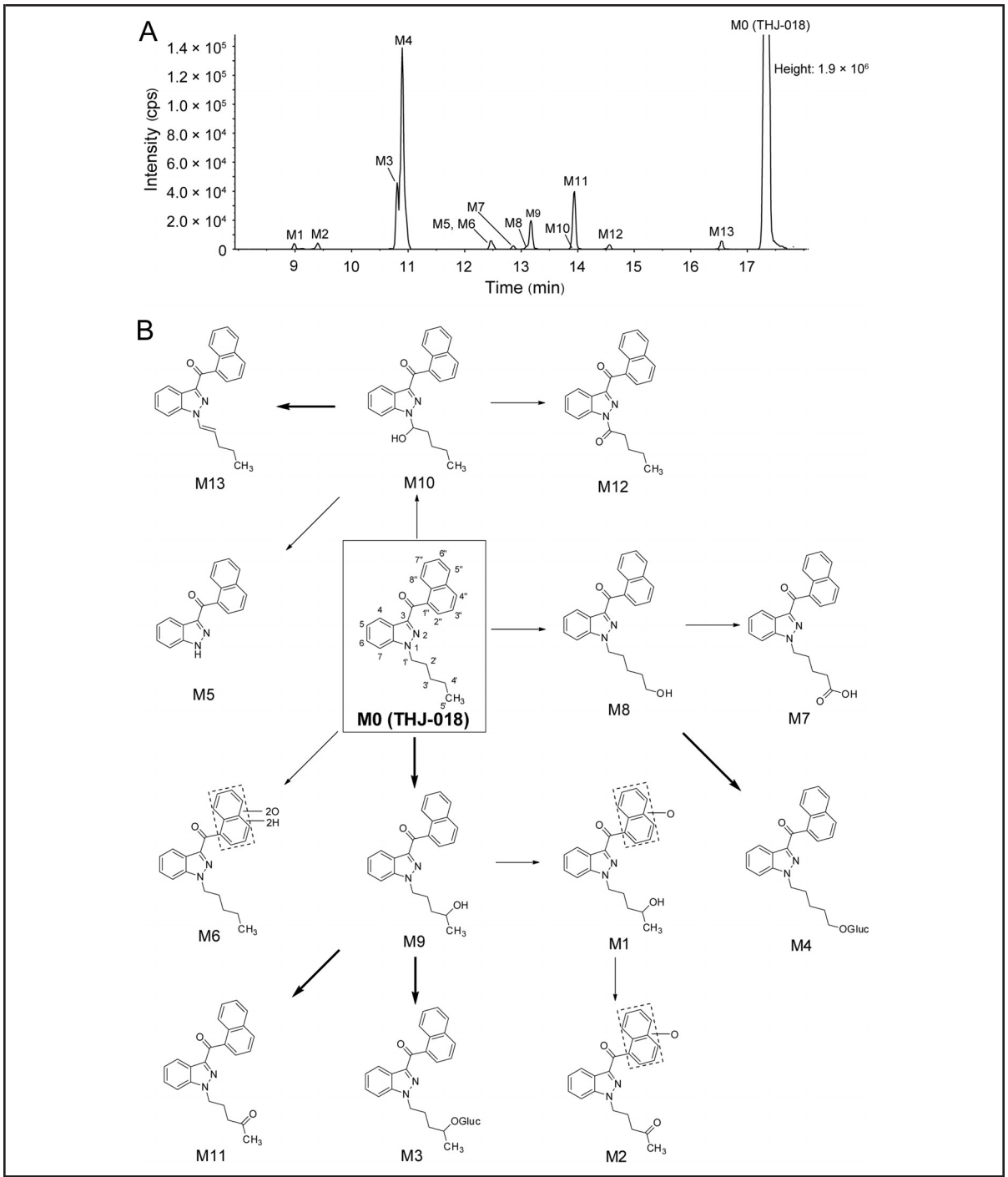

Fig. 2. Metabolic profile (A) and proposed metabolic pathway (B) of THJ-018 after 3-h incubation in human hepatocytes.
Gluc, glucuronide.

ments *m*/*z* 229.0967 and 85.0663 suggested pentyl chain carbonylation (Fig. 3D). 4′-Carbonylation products also were major metabolites of drugs with aliphatic side chain such as 3-*n*-butylphthalide and sameridine *(22, 24)*. Metabolite M1 shared fragments *m*/*z* 145.0399, 213.1017, and 231.1128 with M9 (Fig. 3A), implying pentyl chain hydroxylation; fragment *m*/*z* 171.0450 was 15.9970 Da greater than *m*/*z* 155.0480 of M9, indicating another hydroxylation on naphthalene. M1 also underwent carboxylation to M2, indicated by *m*/*z* 229.0973 and 85.0661.

Table 1. Identification of THJ-018 metabolites after 3-h incubation with human hepatocytes.[a]

ID	Metabolic pathway	Retention time (min)	Mass (*m/z*)	Mass error (ppm)	Formula	Major product ions	MS area	Rank
M1	Dihydroxylation	8.98	375.1708	1.2	$C_{23}H_{22}N_2O_3$	357, 231, 213, 171, 145	1.52×10^4	7
M2	Carbonylation + naphthalene hydroxylation	9.40	373.1559	3.3	$C_{23}H_{20}N_2O_3$	229, 145, 85	1.61×10^4	6
M3	Hydroxylation + glucuronidation	10.81	535.2085	1.8	$C_{29}H_{30}N_2O_8$	359, 341, 231, 213, 155, 145	1.65×10^5	2
M4	Hydroxylation + glucuronidation	10.90	535.2080	1.0	$C_{29}H_{30}N_2O_8$	359, 341, 231, 213, 155, 145	5.63×10^5	1
M5	*N*-Depentylation ($-C_5H_{10}$)	12.45	273.1007	−5.7	$C_{18}H_{12}N_2O$	145, 117	1.42×10^4	9
M6	Dihydrodiol formation on naphthalene	12.50	377.1867	1.9	$C_{23}H_{24}N_2O_3$	289, 215, 145	1.27×10^4	11
M7	Carboxylation	12.86	373.1557	2.8	$C_{23}H_{20}N_2O_3$	355, 327, 227, 217, 155, 127	8.77×10^3	12
M8	Hydroxylation	13.08	359.1771	4.7	$C_{23}H_{22}N_2O_2$	341, 231, 213, 155, 145, 127, 69	7.72×10^3	13
M9	Hydroxylation	13.17	359.1763	2.5	$C_{23}H_{22}N_2O_2$	341, 231, 213, 155, 145, 127, 69	7.26×10^4	4
M10	Hydroxylation	13.87	359.1762	2.3	$C_{23}H_{22}N_2O_2$	341, 231, 213, 155, 145, 127, 69	1.45×10^4	8
M11	Carbonylation	13.94	357.1603	1.5	$C_{23}H_{20}N_2O_2$	229, 155, 145, 127, 85	1.54×10^5	3
M12	Carbonylation	14.57	357.1614	4.6	$C_{23}H_{20}N_2O_2$	273, 229, 145, 127, 85	1.29×10^4	10
M13	Dehydrogenation	16.55	341.1670	6.2	$C_{23}H_{20}N_2O$	213, 155, 145, 127, 69	2.24×10^4	5
M0	Parent	17.34	343.1810	1.4	$C_{23}H_{22}N_2O$	215, 155, 145, 127, 117, 71	7.65×10^6	

[a] Product ions are expressed in nominal *m/z* values because of space limitations.

1′-HYDROXYLATION AND FURTHER DEHYDROGENATION, DEHYDRATION, AND DEALKYLATION

Besides 5′- and 4′-carbons, the heteroatom 1′-carbon was susceptible to hydroxylation, resulting in M10. Fragments *m/z* 231.1123, 155.0493, and 145.0398 suggested pentyl chain hydroxylation. In silico prediction further supported M10 being 1′-OH-THJ-018 (50% probability score). Subsequent M10 oxidation led to the *N*-dealkylation metabolite M5. *N*-Depentylation was observed for several SCs, including JWH-018 *(25)*, AM2201 *(12)*, and UR-144 *(12)*.

M10 also underwent carboxylation, yielding M12 (1′-carbonyl-THJ-018). Fragments *m/z* 229.0979 and 85.0644 indicated pentyl chain carbonylation. Intense *m/z* 273.1017 betrays 1′-carbonylation, in which case the amido bond cleaves easily *(5, 19, 26)*. M13 was the most lipophilic metabolite, eluting at 16.55 min. Characteristic fragments *m/z* 213.1024 and 69.0716 suggested pentyl chain dehydrogenation (Fig. 3E). M13 was probably generated via dehydration of M10, which agreed well with prediction of pent-1′-enyl-THJ-018 (see online Supplemental Table 1) in terms of largest logD4 value.

DIHYDRODIOL FORMATION

M6 produced fragments *m/z* 215.1175 and 145.0399, implying that the indazole and pentyl chain were unchanged. Fragment *m/z* 215.1175 was generated via neutral loss of 162.0692, 34.0068 Da (+2O+2H) larger than naphthalene, from *m/z* 377.1867, suggesting dihydrodiol formation on naphthalene.

THJ-018 IN SILICO PREDICTION

MetaSite predicted 7 first-generation and 4 second-generation metabolites. Online Supplemental Table 1 shows predicted metabolites with probability score, bio-

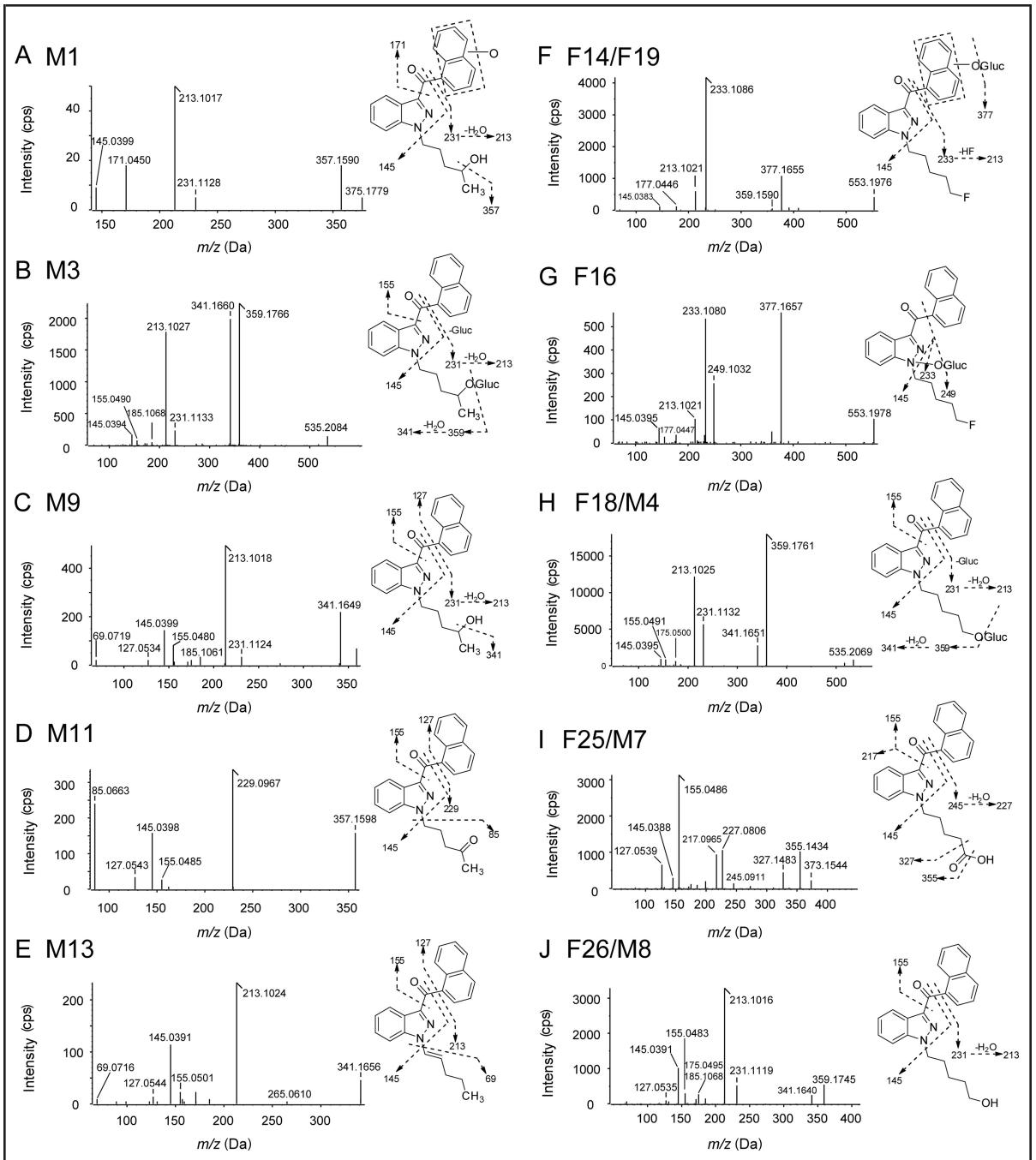

Fig. 3. Product ion spectra and tentative fragmentation patterns for the major metabolites of THJ-018 (A–E) and THJ-2201 (F–J) after incubation with human hepatocytes.

transformation, monoisotopic mass, and calculated logD4. LogD4 for THJ-018 is 6.43. The top 5 predicted metabolites were 4′-OH-THJ-018, 1′-OH-THJ-018, *N*-dependyl-THJ-018, pent-1′-enyl-THJ-018, and 1′-carbonyl-THJ-018.

THJ-2201 METABOLITES IN HEPATOCYTES

Table 2 and Fig. 4 summarize the 27 THJ-2201 metabolites identified in hepatocyte samples. THJ-2201 metabolites were labeled "F" (to distinguish from THJ-018) in order of increasing retention time.

Table 2. Identification of THJ-2201 metabolites after 3-h incubation with human hepatocytes.

ID	Metabolic pathway	Retention time (min)	Mass (*m/z*)	Mass error (ppm)	Formula	Major product ions	MS area	Rank
F1	Oxidative defluorination + hydroxylation + glucuronidation	8.05	551.2017	−1.2	$C_{29}H_{30}N_2O_9$	375, 357, 231, 213, 145	2.88×10^4	15
F2	Oxidative defluorination to COOH + naphthalene hydroxylation	8.45	389.1505	2.4	$C_{23}H_{20}N_2O_4$	371, 343, 227, 217, 171, 161, 145	2.36×10^4	19
F3	Oxidative defluorination + hydroxylation + glucuronidation	8.63	551.2039	2.7	$C_{29}H_{30}N_2O_9$	375, 231, 213, 145	2.64×10^4	17
F4	Oxidative defluorination + hydroxylation + glucuronidation	8.73	551.2058	6.1	$C_{29}H_{30}N_2O_9$	375, 357, 231, 213	1.65×10^4	22
F5	Oxidative defluorination to COOH + naphthalene hydroxylation	8.98	389.1502	1.6	$C_{23}H_{20}N_2O_4$	371, 343, 245, 227, 217, 171, 145	1.10×10^5	7
F6	Oxidative defluorination to COOH + dihydrodiol formation on naphthalene	8.99	407.1597	−1.1	$C_{23}H_{22}N_2O_5$	389, 371, 343, 245, 227, 217, 171, 145, 143	9.72×10^3	26
F7	Oxidative defluorination + naphthalene hydroxylation	9.02	375.1709	1.5	$C_{23}H_{22}N_2O_3$	357, 231, 213, 175, 171, 145, 69	6.65×10^4	11
F8	Oxidative defluorination + dihydrodiol formation on naphthalene	9.02	393.1808	−0.2	$C_{23}H_{24}N_2O_4$	375, 357, 231, 213, 175, 171, 145	5.16×10^4	13
F9	Oxidative defluorination + naphthalene dihydroxylation + glucuronidation	9.32	567.1968	−0.8	$C_{29}H_{30}N_2O_{10}$	391, 373, 231, 213, 187, 145	2.27×10^4	20
F10	Oxidative defluorination to COOH + naphthalene hydroxylation	9.38	389.1475	−5.4	$C_{23}H_{20}N_2O_4$	371, 343, 245, 227, 217, 171, 145	9.01×10^3	27
F11	Oxidative defluorination + hydroxylation + glucuronidation	9.59	551.2024	0.1	$C_{29}H_{30}N_2O_9$	375, 357, 231, 213, 171, 145	2.68×10^4	16
F12	Oxidative defluorination + naphthalene dihydroxylation + glucuronidation	9.61	567.1948	−4.4	$C_{29}H_{30}N_2O_{10}$	391, 231, 213, 145	2.64×10^4	18
F13	Naphthalene hydroxylation	10.02	377.1667	2.0	$C_{23}H_{21}N_2O_2F$	289, 233, 213, 177, 145, 69	7.6×10^4	9
F14	Naphthalene hydroxylation + glucuronidation	10.20	553.1987	1.2	$C_{29}H_{29}N_2O_8F$	377, 359, 233, 213, 177, 145	2.09×10^5	4
F15	Hydroxylation + glucuronidation	10.71	553.1990	1.8	$C_{29}H_{29}N_2O_8F$	377, 359, 249, 231, 155, 145	7.05×10^4	10
F16	*N*-Oxide + glucuronidation	10.86	553.1973	−1.4	$C_{29}H_{29}N_2O_8F$	377, 359, 249, 233, 213, 177, 145	1.27×10^5	5
F17	Naphthalene dihydroxylation + glucuronidation	10.91	569.1903	−4.7	$C_{29}H_{29}N_2O_9F$	393, 233, 213, 177, 145, 69	1.62×10^4	23
F18	Oxidative defluorination + glucuronidation	10.94	535.2078	0.5	$C_{29}H_{30}N_2O_8$	359, 341, 231, 213, 175, 155, 145	2.53×10^6	1
F19	Naphthalene hydroxylation + glucuronidation	11.12	553.1977	−0.7	$C_{29}H_{29}N_2O_8F$	377, 233, 213, 145	1.10×10^5	6
F20	Naphthalene dihydroxylation + glucuronidation	11.12	569.1918	−2.1	$C_{29}H_{29}N_2O_9F$	393, 233, 213, 145, 69	7.84×10^4	8
F21	Dihydrodiol formation on naphthalene	11.16	395.1747	−4.7	$C_{23}H_{23}N_2O_3F$	377, 289, 233, 213, 177, 145, 69	1.23×10^4	24
F22	*N*-Oxide	11.20	377.1661	0.4	$C_{23}H_{21}N_2O_2F$	289, 249, 233, 213, 177, 145, 161, 145	1.82×10^4	21
F23	Naphthalene dihydroxylation + glucuronidation	11.27	569.1932	0.4	$C_{29}H_{29}N_2O_9F$	393, 233, 213, 177, 145	3.01×10^4	14
F24	*N*-Dealkylation ($-C_5H_9F$)	12.43	273.1017	−1.9	$C_{18}H_{12}N_2O$	145, 117, 90	5.67×10^4	12
F25	Oxidative defluorination to COOH	12.86	373.1542	−1.4	$C_{23}H_{20}N_2O_3$	355, 327, 245, 227, 217, 155, 145, 127	3.85×10^5	3
F26	Oxidative defluorination	13.08	359.1747	−1.9	$C_{23}H_{22}N_2O_2$	341, 231, 213, 185, 175, 155, 145, 127	5.40×10^5	2
F27	Hydroxylation	13.31	377.1673	3.4	$C_{23}H_{21}N_2O_2F$	359, 249, 231, 177, 155, 145, 127	1.14×10^4	25
F0	Parent	15.73	361.1709	−0.4	$C_{23}H_{21}N_2OF$	233, 213, 185, 177, 155, 145, 69	2.16×10^6	

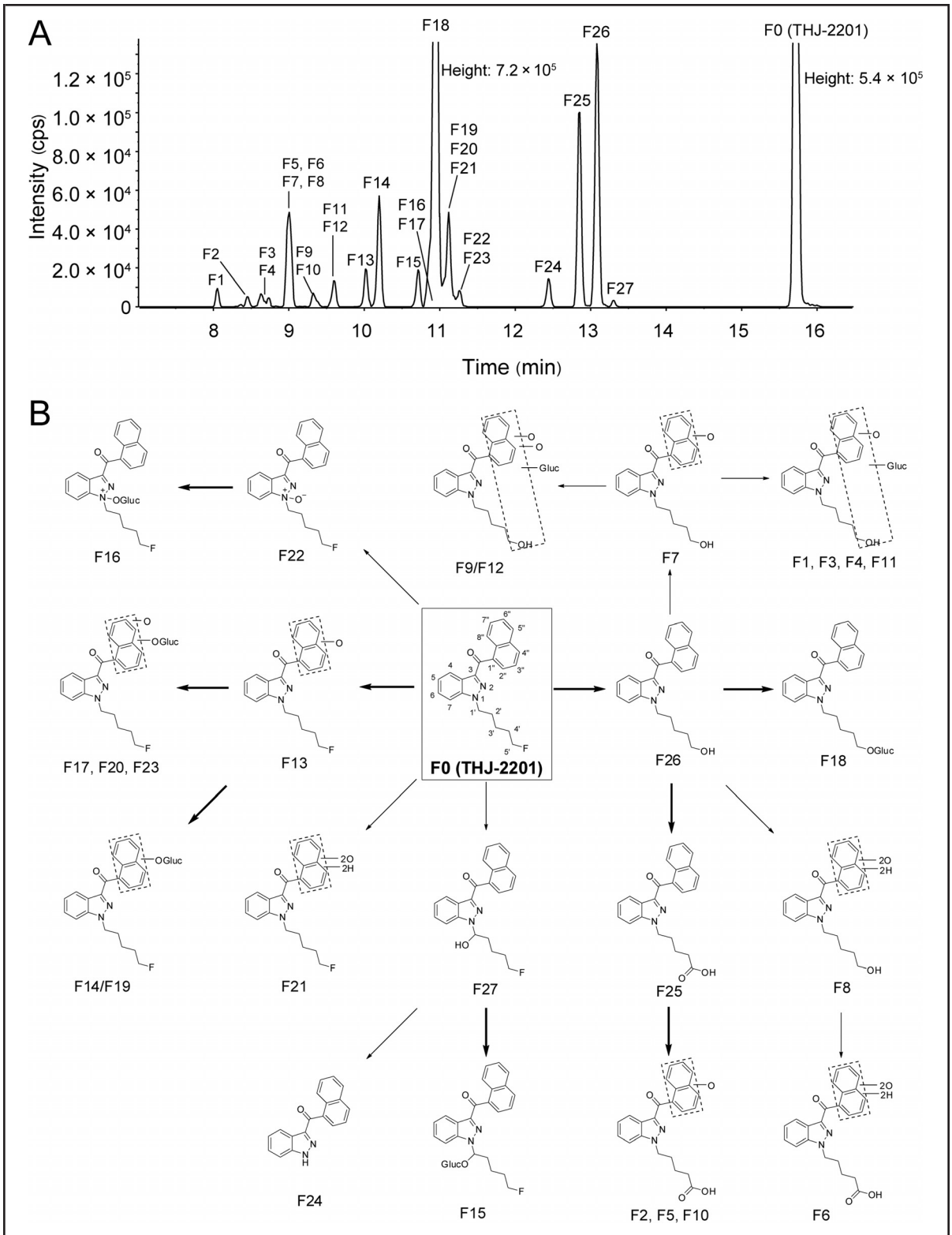

Fig. 4. **Metabolic profile (A) and proposed metabolic pathway (B) of THJ-2201 after 3-h incubation in human hepatocytes.**
Gluc, glucuronide.

MAJOR THJ-2201 METABOLITES

On the basis of peak areas, primary metabolites were 5′-OH-THJ-018 glucuronide (F18), 5′-OH-THJ-018 (F26), THJ-018 pentanoic acid (F25), and glucuronides of monooxide (F14, F16, and F19). Their product ion spectra and fragmentation are shown in Fig. 3, F–J. Product ion spectra of other metabolites are shown in online Supplemental Fig. 2.

OXIDATIVE DEFLUORINATION AND FURTHER OXIDATION AND GLUCURONIDATION

For F26, precursor *m*/*z* 359.1745 and fragment *m*/*z* 231.1119 were 1.9971 Da (−F+OH) less than corresponding THJ-2201 ions (Fig. 3J), implying oxidative defluorination. Other F26 fragments *m*/*z* 213.1016, 155.0483, and 145.0391 suggested that indazole and naphthalene moieties were unmodified. Tentatively, F26 was proposed as 5′-OH-THJ-018. F26 was further glucuronidated to 5′-OH-THJ-018 glucuronide (F18), whose intense fragment *m*/*z* 359.1761 was formed via loss of glucuronide, with other fragments the same as F26 (Fig. 3H).

F26 (5′-OH-THJ-018) underwent naphthalene hydroxylation, yielding F7, indicated by fragments *m*/*z* 231.1128, 213.1019, 175.0466, 171.0437, and 145.0384. F7 and its isomers, which were not identified themselves, were further glucuronidated to yield F1/F3/F4/F11. These conjugates yielded similar product ion spectra and displayed *m*/*z* 375.1698 via loss of glucuronide. Other fragments remained the same as F7. Additionally, F7 could undergo another hydroxylation on naphthalene and glucuronidation yielding F9/F12, which shared fragments *m*/*z* 231.1126, 213.1021, and 145.0405 with F7. Neutral glucuronide losses from F9/F12 led to *m*/*z* 391.1655, 15.9946 Da larger than *m*/*z* 375.1709 of F7, indicating F9/F12 being glucuronides of hydroxylated F7.

Carboxylation of F26 (5′-OH-THJ-018) yielded THJ-018 pentanoic acid (F25), displaying the same retention time and fragment profile as M7 of THJ-018 (Fig. 3I). Further hydroxylation of F25 generated F2/F5/F10. Characteristic carboxylic acid ions, *m*/*z* 227.0806 and 217.0971, were observed; in addition, their fragment *m*/*z* 171.0434 indicated naphthalene hydroxylation.

Dihydrodiol metabolites of 5′-OH-THJ-018 (F26) and THJ-018 pentanoic acid (F25), namely F8 and F6, were detected. F8 shared fragments *m*/*z* 231.1125, 213.1018, and 145.0394 with F26; its fragment *m*/*z* 231.1125 was generated by characteristic neutral loss of 162.0683 Da, corresponding to naphthalene dihydrodiol as described for M6. This particular neutral loss also was observed for F6.

1′-HYDROXYLATION AND FURTHER GLUCURONIDATION AND DEALKYLATION

Similar to THJ-018, 1′-hydroxylation also was observed for THJ-2201 (F27). Its fragments *m*/*z* 155.0488 and 145.0393 were the same as for THJ-2201; *m*/*z* 249.1031 was 15.9942 Da more than *m*/*z* 233.1089 of THJ-2201, indicating pentyl chain hydroxylation. MetaSite predicted 1′-OH-THJ-2201 with a 100% probability score. We tentatively assigned F27 as 1′-OH-THJ-2201. Further glucuronidation yielded 1′-OH-THJ-2201 glucuronide (F15). *N*-Dealkylation metabolite F24 was equivalent to M5 in terms of the same retention time and product ion spectrum.

NAPHTHALENE HYDROXYLATION AND FURTHER GLUCURONIDATION

Naphthalene hydroxylation formed F13. Its fragments *m*/*z* 233.1082, 213.1015, 177.0445, 145.0393, and 69.0725 were the same as for THJ-2201; *m*/*z* 289.0947 suggested naphthalene hydroxylation. Neutral loss of glucuronide from F14/F19 generated *m*/*z* 377.1655 (Fig. 3F); fragments *m*/*z* 233.1086, 213.1021, and 145.0383 were the same as F13. Thus, F14/F19 were proposed as F13 glucuronides. F13 could undergo a second naphthalene hydroxylation and further glucuronidation, yielding F17/F20/F23, indicated by fragments *m*/*z* 393.1617, 233.1084, 213.1021, 177.0434, and 145.0396.

N-OXIDE AND FURTHER GLUCURONIDATION

We observed *N*-oxide of THJ-2201 (F22) followed by glucuronidation. F22 shared fragments *m*/*z* 233.1079, 213.1018, 177.0444, and 145.0397 with THJ-2201, indicating 5-fluoropentyl chain and indazole unmodified. However, fragments *m*/*z* 249.1026 and 161.0338 were 15.9947 Da more than *m*/*z* 233.1079 and 145.0397, respectively, pointing to indazole monooxidation. F22 was probably an *N*-oxide rather than a hydroxylated metabolite, under which circumstance it is unlikely to yield high abundance of *m*/*z* 249.1026 and 233.1079 simultaneously. Generally, neutral loss of H_2O, rather than O, is observed between fragment ions of hydroxylated metabolites, whereas loss of O or OH radical is common for *N*-oxides during fragmentation *(27–29)*.

F16 is probably F22 glucuronide, since it also showed concurrent appearance of *m*/*z* 249.1032 and 233.1080. Although unusual, *N*-oxide glucuronidation is important in the metabolism of some xenobiotics, e.g., the antidepressant vortioxetine *(28)* and anticonvulsants GI265080 and GW273293 *(30)*.

DIHYDRODIOL FORMATION

The naphthalene dihydrodiol metabolite of THJ-2201 (F21) shares fragments *m*/*z* 233.1079, 213.1016, 177.0458, and 145.0395 with THJ-2201; *m*/*z* 233.1079

was generated by a particular 162.0685 Da neutral loss, corresponding to naphthalene dihydrodiol.

THJ-2201 IN SILICO PREDICTION

MetaSite predicted 8 first-generation metabolites and 7 second-generation metabolites. Online Supplemental Table 1 details predicted metabolites. The logD4 value of THJ-2201 is 5.96. The top 4 predicted metabolites were *N*-dependyl-THJ-018, 1′-OH-THJ-2201, 1′-carbonyl-THJ-2201, and pent-1′-enyl-THJ-2201.

Discussion

HLM METABOLIC STABILITY

In vitro $T_{1/2}$ and CL_{int} estimate a drug's susceptibility to metabolism and facilitate in vivo CL_H, in vivo $T_{1/2}$, and bioavailability prediction *(21)*. THJ-018 and THJ-2201 CL_{int} and ER indicate that they are intermediate- and fast-metabolizing drugs, respectively *(31, 32)*. $T_{1/2}$ and CL_{int} are useful for future predictions of human pharmacokinetics once plasma protein binding and volume of distribution are determined.

IN SILICO PREDICTIONS

In silico prediction assists metabolite identification without reference standards. MetaSite mainly focuses on CYP450-catalyzed metabolism and does not simulate reactions mediated by non-CYP450 oxidases such as aldehyde oxidase *(33)*. Despite this limitation, predicted THJ-018 metabolites are in good agreement with hepatocyte metabolites: all top 5 predicted metabolites were detected. However, the overall performance of MetaSite was not as accurate for THJ-2201 as for THJ-018 because of strong underestimation on oxidative defluorination (14.1% probability score), probably because the reaction was not catalyzed by CYP450.

THJ-018 AND THJ-2201 METABOLISM COMPARED WITH JWH-018 AND AM-2201

THJ-018 is metabolized similarly to JWH-018. Pentyl chain hydroxylation and further glucuronidation, carboxylation, and naphthalene dihydrodiol formation were detected for both *(11, 14)*. However, susceptibility to metabolism was different for indole (JWH-018) and indazole (THJ-018) rings. For JWH-018, several indole-hydroxylated metabolites were identified *(11)*, whereas for THJ-018, we did not detect any indazole-hydroxylated metabolite. This might be attributed to electron cloud distribution differences between indole and indazole rings. Likewise, no indazole-hydroxylated metabolites were observed for AKB-48 and AB-PINACA *(19, 34)*. Both AM-2201 and THJ-2201 underwent oxidative defluorination with subsequent carboxylation and glucuronidation *(11, 16)*. Surprisingly, an uncommon pathway was observed for THJ-2201, i.e., glucuronidation after *N*-oxidation (F16). *N*-Oxide glucuronidation is rare, with only sporadic reports *(28, 30)*. To date, this reaction was not reported for any other SC.

THJ-018 AND THJ-2201 SHARED METABOLITES

Coeluting isomers are difficult to distinguish. For THJ-018, we detected isomers M8 (5′-OH-THJ-018) and M9 (4′-OH-THJ-018) as well as M4 (5′-OH-THJ-018 glucuronide) and M3 (4′-OH-THJ-018 glucuronide). However, for THJ-2201, we detected F26 (5′-OH-THJ-018) and F18 (5′-OH-THJ-018 glucuronide) only after oxidative defluorination. Oxidative defluorination also was the primary metabolic pathway for fluorinated SC, such as AM-2201 *(16)*, 5F-AB-PINACA *(19)*, XLR-11 *(35)*, and 5F-PB-22 *(36)*, and it dominated THJ-2201 metabolism. F26 and F18 have retention times and spectra identical to those of M8 and M4, respectively. Therefore, M8 and M4 were assigned as 5′-OH-THJ-018 and 5′-OH-THJ-018 glucuronide, respectively; then M9 and M3 were proposed as 4′-OH-THJ-018 and 4′-OH-THJ-018 glucuronide.

After oxidative defluorination, THJ-2201 produced several THJ-018 metabolites. Further carboxylation and glucuronidation led to the same metabolites, namely, F25/M7 and F18/M4.

SPECIFIC MARKERS FOR DOCUMENTING THJ-018 AND THJ-2201 INTAKE

As discussed above, unambiguous identification of THJ-018 or THJ-2201 consumption cannot be achieved by monitoring 5′-OH-THJ-018, THJ-018 pentanoic acid, and 5′-OH-THJ-018 glucuronide. It may be essential for legal purposes to identify which substance is consumed because of different legal statuses. Metabolites containing fluoropentyl chain should be used to distinguish THJ-2201 from THJ-018 intake. To verify consumption of THJ-018 or THJ-2201 or both, 5′-OH-THJ-018 (M8/F26) and THJ-018 pentanoic acid (M7/F25) should be observed at high abundance. On the basis of our hepatocyte study, specific markers for THJ-2201 consumption include naphthalene hydroxylated THJ-2201 (F13), *N*-oxide THJ-2201 (F22), and 1′-OH-THJ-2201 (F27). Unique markers for THJ-018 consumption include 4′-OH-THJ-018 (M9), 4′-carbonyl-THJ-018 (M11), pent-1′-enyl-THJ-018 (M13), and 1′-OH-THJ-018 (M10). Of note, 4′-OH-THJ-018 (THJ-018 specific) and 5′-OH-THJ-018 (shared) possessed similar physicochemical properties, making complete chromatographic separation challenging. However, chromatographic resolution of these 2 THJ-018 hydroxypentyl isomers might be important for distinguishing THJ-018 and THJ-2201 intake, similar to observations for JWH-018 and AM-2201 *(14, 16, 37)*. THJ-2201 produced abundant 5′-OH-THJ-018 and no 4′-OH-THJ-018, whereas THJ-018

produced comparable amounts of 4′-OH-THJ-018 and 5′-OH-THJ-018. Distinguishing THJ-2201 intake from THJ-018 can be accomplished by simultaneous screening of metabolites retaining fluorine or via ratios of 4′-OH-THJ-018 and 5′-OH-THJ-018.

Urine is the most common drug detection matrix because of adequate sample volume and high drug concentrations compared with blood; hence the importance of identifying urinary metabolites as targets. When extrapolating from hepatocytes to urine, some factors, such as extrahepatic metabolism, transporters, and metabolites' enrichment in urine, may affect the relative abundance of urinary metabolites, and thus, selection of identifying markers. Extrahepatic formation of glucuronide- and sulfate-acetaminophen in anhepatic model rats accounted for about 28% of metabolites formed in normal control rats *(38)*. Selective hepatic uptake of different metabolites by transporter organic anion-transporting polypeptide 2B1 led to unique urinary distribution of scutellarin metabolites *(39)*. Urinary metabolite abundance profiles may not represent the hepatic metabolic scenario if feces is the major excretion route instead of urine *(40)*. For these reasons, it would be preferable to obtain authentic THJ-018 and THJ-2201 urine samples to confirm that major hepatocyte metabolites match urinary metabolites. However, such samples are not currently available to us despite our efforts.

These metabolism results also are important for assessing pharmacodynamic effects. Major hydroxylated JWH-018 and AM-2201 metabolites such as 4′-OH-JWH-018, 5′-OH-JWH-018, and 4′-OH-AM-2201 remained full agonists at nanomolar concentrations *(11, 16)*. Because of structural similarity, high binding affinity and activity can be expected for hydroxypentyl THJ-018 and THJ-2201 metabolites, which may prolong or even enhance the adverse effects of THJ-018 and THJ-2201.

In summary, for the first time, we characterized human metabolism of THJ-018 and THJ-2201 by HR-MS in human hepatocytes. HR-MS provided robust data acquisition and processing capability, facilitating expedient identification of optimal metabolite targets. These data empower clinical laboratories to target markers of NPS intake and manufacturers to focus synthesis efforts on the most appropriate targets. These data also enable linkage of adverse events to specific NPSs and the knowledge to educate the public on the dangers of specific NPSs. Our analysis strategy, HR-MS data acquisition and processing and hepatocyte incubation, is also applicable to further studies of newly emerging NPSs.

Author Contributions: *All authors confirmed they have contributed to the intellectual content of this paper and have met the following 3 requirements: (a) significant contributions to the conception and design, acquisition of data, or analysis and interpretation of data; (b) drafting or revising the article for intellectual content; and (c) final approval of the published article.*

Authors' Disclosures or Potential Conflicts of Interest: *Upon manuscript submission, all authors completed the author disclosure form. Disclosures and/or potential conflicts of interest:*

Employment or Leadership: None declared.
Consultant or Advisory Role: None declared.
Stock Ownership: None declared.
Honoraria: None declared.
Research Funding: The Intramural Research Program (IRP) of the National Institute on Drug Abuse, NIH. The Molecular Discovery Company provided the MetaSite software.
Expert Testimony: None declared.
Patents: None declared.

Role of Sponsor: The funding organizations played no role in the design of study, choice of enrolled patients, review and interpretation of data, or preparation or approval of manuscript.

References

1. Castaneto MS, Gorelick DA, Desrosiers NA, Hartman RL, Pirard S, Huestis MA. Synthetic cannabinoids: epidemiology, pharmacodynamics, and clinical implications. Drug Alcohol Depend 2014;144:12–41.
2. Desrosiers NA, Lee D, Concheiro-Guisan M, Scheidweiler KB, Gorelick DA, Huestis MA. Urinary cannabinoid disposition in occasional and frequent smokers: is THC-glucuronide in sequential urine samples a marker of recent use in frequent smokers? Clin Chem 2014;60:361–72.
3. Hermanns-Clausen M, Kneisel S, Szabo B, Auwarter V. Acute toxicity due to the confirmed consumption of synthetic cannabinoids: clinical and laboratory findings. Addiction 2013;108:534–44.
4. Seely KA, Lapoint J, Moran JH, Fattore L. Spice drugs are more than harmless herbal blends: a review of the pharmacology and toxicology of synthetic cannabinoids. Prog Neuropsychopharmacol Biol Psychiatry 2012;39:234–43.
5. Uchiyama N, Shimokawa Y, Kawamura M, Kikura-Hanajiri R, Hakamatsuka T. Chem analysis of a benzofuran derivative, 2-(2-ethylaminopropyl)benzofuran (2-EAPB), eight synthetic cannabinoids, five cathinone derivatives, and five other designer drugs newly detected in illegal products. Forensic Toxicol 2014;32:266–81.
6. Shevyrin V, Melkozerov V, Nevero A, Eltsov O, Morzherin Y, Shafran Y. 3-Naphthoylindazoles and 2-naphthoylbenzoimidazoles as novel chemical groups of synthetic cannabinoids: chemical structure elucidation, analytical characteristics and identification of the first representatives in smoke mixtures. Forensic Sci Int 2014;242:72–80.
7. US Department of Justice. Schedules of controlled substances: temporary placement of three synthetic cannabinoids into Schedule I. Fed Regist 2015:5042–7.
8. Uchiyama N, Shimokawa Y, Matsuda S, Kawamura M, Kikura-Hanajiri R, Goda Y. Two new synthetic cannabinoids, AM-2201 benzimidazole analog (FUBIMINA) and (4-methylpiperazin-1-yl)(1-pentyl-1H-indol-3-yl)methanone (MEPIRAPIM), and three phenethylamine derivatives, 25H-NBOMe 3,4,5-trimethoxybenzyl analog, 25B-NBOMe, and 2C-N-NBOMe, identified in illegal products. Forensic Toxicol 2014;32:105–15.
9. Drugs-Forum. 2014. https://drugs-forum.com/forum/showthread.php?t=231444&page=2 (Accessed December 2014).
10. National Institute of Health Sciences. Data Search System for New Psychoactive Substances. 2015. http://npsdb.nihs.go.jp/Search/Default_e.aspx (Accessed March 2015).
11. Chimalakonda KC, Seely KA, Bratton SM, Brents LK, Moran CL, Endres GW, et al. Cytochrome P450-mediated oxidative metabolism of abused synthetic cannabinoids found in K2/Spice: identification of novel cannabinoid receptor ligands. Drug Metab Dispos 2012;40:2174–84.
12. Sobolevsky T, Prasolov I, Rodchenkov G. Detection of urinary metabolites of AM-2201 and UR-144, two novel synthetic cannabinoids. Drug Test Anal 2012;

4:745–53.
13. Desrosiers NA, Himes SK, Scheidweiler KB, Concheiro-Guisan M, Gorelick DA, Huestis MA. Phase I and II cannabinoid disposition in blood and plasma of occasional and frequent smokers following controlled smoked cannabis. Clin Chem 2014;60:631–43.
14. Wintermeyer A, Moller I, Thevis M, Jubner M, Beike J, Rothschild MA, Bender K. In vitro phase I metabolism of the synthetic cannabimimetic JWH-018. Anal Bioanal Chem 2010;398:2141–53.
15. Hutter M, Broecker S, Kneisel S, Auwarter V. Identification of the major urinary metabolites in man of seven synthetic cannabinoids of the aminoalkylindole type present as adulterants in 'herbal mixtures' using LC-MS/MS techniques. J Mass Spectrom 2012;47:54–65.
16. Hutter M, Moosmann B, Kneisel S, Auwarter V. Characteristics of the designer drug and synthetic cannabinoid receptor agonist AM-2201 regarding its chemistry and metabolism. J Mass Spectrom 2013;48:885–94.
17. Zhu M, Zhang H, Humphreys WG. Drug metabolite profiling and identification by high-resolution mass spectrometry. J Biol Chem 2011;286:25419–25.
18. Diao X, Pang X, Xie C, Guo Z, Zhong D, Chen X. Bioactivation of 3-n-butylphthalide via sulfation of its major metabolite 3-hydroxy-NBP: mediated mainly by sulfotransferase 1A1. Drug Metab Dispos 2014; 42:774–81.
19. Wohlfarth A, Castaneto MS, Zhu M, Pang S, Scheidweiler KB, Kronstrand R, Huestis MA. Pentylindole/pentylindazole synthetic cannabinoids and their 5-fluoro analogs produce different primary metabolites: metabolite profiling for AB-PINACA and 5F-AB-PINACA. AAPS J 2015;17:660–77.
20. Harris CR, Brown A. Synthetic cannabinoid intoxication: a case series and review. J Emerg Med 2013;44: 360–6.
21. Baranczewski P, Stanczak A, Sundberg K, Svensson R, Wallin A, Jansson J, et al. Introduction to in vitro estimation of metabolic stability and drug interactions of new chemical entities in drug discovery and development. Pharmacol Rep 2006;58:453–72.
22. Diao X, Deng P, Xie C, Li X, Zhong D, Zhang Y, Chen X. Metabolism and pharmacokinetics of 3-n-butylphthalide (NBP) in humans: the role of cytochrome P450s and alcohol dehydrogenase in biotransformation. Drug Metab Dispos 2013;41:430–44.
23. Deng P, You T, Chen X, Yuan T, Huang H, Zhong D. Identification of amiodarone metabolites in human bile by ultraperformance liquid chromatography/quadrupole time-of-flight mass spectrometry. Drug Metab Dispos 2011;39:1058–69.
24. Sohlenius-Sternbeck AK, Chelpin HV, Orzechowski A, Halldin MM. Metabolism of sameridine to monocarboxylated products by hepatocytes isolated from the male rat. Drug Metab Dispos 2000;28:695–700.
25. Grigoryev A, Savchuk S, Melnik A, Moskaleva N, Dzhurko J, Ershov M, et al. Chromatography-mass spectrometry studies on the metabolism of synthetic cannabinoids JWH-018 and JWH-073, psychoactive components of smoking mixtures. J Chromatogr B Analyt Technol Biomed Life Sci 2011;879:1126–36.
26. Beckett AH. Metabolic oxidation of aliphatic basic nitrogen atoms and their alpha-carbon atoms. Xenobiotica 1971;1:365–83.
27. Ding J, Chen X, Gao Z, Dai X, Li L, Xie C, et al. Metabolism and pharmacokinetics of novel selective vascular endothelial growth factor receptor-2 inhibitor apatinib in humans. Drug Metab Dispos 2013;41:1195–210.
28. Uldam HK, Juhl M, Pedersen H, Dalgaard L. Biosynthesis and identification of an N-oxide/N-glucuronide metabolite and first synthesis of an N-O-glucuronide metabolite of Lu AA21004. Drug Metab Dispos 2011;39: 2264–74.
29. Ibrahim H, Couderc F, Perio P, Collin F, Nepveu F. Behavior of N-oxide derivatives in atmospheric pressure ionization mass spectrometry. Rapid Commun Mass Spectrom 2013;27:621–8.
30. Ismail IM, Dear GJ, Roberts AD, Plumb RS, Ayrtont J, Sweatman BC, Bowers GD. N-O glucuronidation: a major human metabolic pathway in the elimination of two novel anti-convulsant drug candidates. Xenobiotica 2002;32:29–43.
31. McNaney CA, Drexler DM, Hnatyshyn SY, Zvyaga TA, Knipe JO, Belcastro JV, Sanders M. An automated liquid chromatography-mass spectrometry process to determine metabolic stability half-life and intrinsic clearance of drug candidates by substrate depletion. Assay Drug Dev Technol 2008;6:121–9.
32. Lave T, Dupin S, Schmitt C, Valles B, Ubeaud G, Chou RC, et al. The use of human hepatocytes to select compounds based on their expected hepatic extraction ratios in humans. Pharmaceut Res 1997;14:152–5.
33. T'Jollyn H, Boussery K, Mortishire-Smith RJ, Coe K, De Boeck B, Van Bocxlaer JF, Mannens G. Evaluation of three state-of-the-art metabolite prediction software packages (Meteor, MetaSite, and StarDrop) through independent and synergistic use. Drug Metab Dispos 2011;39:2066–75.
34. Gandhi AS, Zhu M, Pang S, Wohlfarth A, Scheidweiler KB, Liu HF, Huestis MA. First characterization of AKB-48 metabolism, a novel synthetic cannabinoid, using human hepatocytes and high-resolution mass spectrometry. AAPS J 2013;15:1091–8.
35. Wohlfarth A, Pang SK, Zhu MS, Gandhi AS, Scheidweiler KB, Liu HF, Huestis MA. First metabolic profile of XLR-11, a novel synthetic cannabinoid, obtained by using human hepatocytes and high-resolution mass spectrometry. Clin Chem 2013;59:1638–48.
36. Wohlfarth A, Gandhi AS, Pang S, Zhu M, Scheidweiler KB, Huestis MA. Metabolism of synthetic cannabinoids PB-22 and its 5-fluoro analog, 5F-PB-22, by human hepatocyte incubation and high-resolution mass spectrometry. Anal Bioanal Chem 2014;406:1763–80.
37. Scheidweiler KB, Huestis MA. Simultaneous quantification of 20 synthetic cannabinoids and 21 metabolites, and semi-quantification of 12 alkyl hydroxy metabolites in human urine by liquid chromatography-tandem mass spectrometry. J Chromatogr A 2014; 1327:105–17.
38. Li XD, Xia SQ, Lv Y, He P, Han J, Wu MC. Conjugation metabolism of acetaminophen and bilirubin in extrahepatic tissues of rats. Life Sci 2004;74:1307–15.
39. Gao C, Zhang H, Guo Z, You T, Chen X, Zhong D. Mechanistic studies on the absorption and disposition of scutellarin in humans: selective OATP2B1-mediated hepatic uptake is a likely key determinant for its unique pharmacokinetic characteristics. Drug Metab Dispos 2012;40:2009–20.
40. Xie C, Zhou J, Guo Z, Diao X, Gao Z, Zhong D, et al. Metabolism and bioactivation of famitinib, a novel inhibitor of receptor tyrosine kinase, in cancer patients. Br J Pharmacol 2013;168:1687–706.